An Optimization Strategy for the Synthesis of Hi-Performance Isophoric Sparse Arrays

Daniele Pinchera
DIEI - University of Cassino and Southern Lazio
CNIT and ELEDIA@UniCAS
via Di Biasio 43, 03043 Cassino, Italy
pinchera@unicas.it

***Abstract*—In this contribution, an effective strategy for the synthesis of equal-amplitude (isophoric) sparse arrays is presented. The approach consists of an iterative procedure starting from a non-equal amplitude layout. The method is very effective, and is demonstrated by an in-depth numerical analysis of a synthesis example.**

***Index Terms*—Radiation pattern synthesis, Antenna Arrays, Optimization techniques**

I. Introduction

The synthesis of antenna arrays is one of the hot topics of applied electromagnetics and, in particular, one of the critical points for achieving the high demands of modern telecommunication systems. Most of the more advanced communications systems rely on arrays of tens or hundreds of radiating elements, and this number will increase in the future [1]–[3].

It is then of paramount importance to investigate the architectures capable of providing the highest performances, possibly reducing the number of control points [4]. Sparse arrays are one of the most efficient architectures in terms of radiating element reduction, and a lot of practical algorithms have been developed for their synthesis in the last years [5]–[11]. Unfortunately, the synthesis of sparse antenna arrays with equal excitations, also known as isophoric arrays [12], still represent an open challenge for antenna engineers.

A novel approach, Isophoric IDEA (I-IDEA) [13], has been recently developed to face this synthesis problem: I-IDEA works as a local optimizer, that starts from an existing solution, but differently from other schemes, in I-IDEA the starting point of the synthesis is a sparse antenna array layout with non-equal amplitude excitations, and the algorithm works towards gradually transforming it into an equal amplitude one.

In this contribution, we will discuss the capability of I-IDEA to generate sparse isophoric arrays allowing high performance also when the beam is steered, using a simple iterative procedure, that progressively refines the isophoric solution found.

II. The I-IDEA synthesis algorithm

The analysis in this document will focus on pencil beams, but the proposed approach can be applied to any specifications that we can write in terms of an arbitrary power pattern mask. Let us now consider that we have already synthesized the layout (element positions and excitations) of an array capable of radiating the wanted pencil beam pattern (with a regular or non-regular lattice): this array of N radiating elements displaced on the $(\mathbf{x};\mathbf{y})$ plane will constitute the starting point of I-IDEA.

If the positions of each element is given by $(x_n; y_n)$, the array factor of this array, at the working frequency f, can be calculated as:

$$AF(u,v) = \sum_{n=1}^{N} c_n e^{j\beta(x_n u + y_n v)} \tag{1}$$

where c_n is the relative excitation of the $n-$th element (a real positive number), $u = \sin\theta\cos\phi$ and $v = \sin\theta\sin\phi$, and $\beta = 2\pi/\lambda$ is the free space wavenumber, with λ the working wavelength, and (θ, ϕ) are the angular coordinates of a standard spherical coordinate system.

The core of I-IDEA is to iteratively modify the positions of the initial sources in order to reduce the excitation dynamic, until all the sources share the same amplitude. To do so three on the sources are iterated: "inflation", "convex optimization" and "deflation".

In the "inflation", each one of the N sources, is *inflated* into a set of $P \geq 2$ sources of coordinates $(\tilde{x}^k_{n,p}; \tilde{y}^k_{n,p})$, displaced at the vertexes of a regular polygon, inscribed in a circle of radius $\delta << \lambda$ (f.i. $\delta = \lambda/100$) with the center in $(x_n; y_n)$:

$$(\tilde{x}^k_{n,p}; \tilde{y}^k_{n,p}) = (x^k_n + \delta\cos(\phi_p + \phi_{n,0}); y^k_n + \delta\sin(\phi_p + \phi_{n,0})) \tag{2}$$

where $\phi_p = 2p\pi/P$ and $\phi_{n,0}$ are inessential offset angles (see Fig.1). Roughly speaking, we substitute the starting array with an array with a larger number of radiators.

Once the array is inflated, we can perform the calculation of the excitations $\tilde{c}^{k+1}_{n,p}$ of the inflated sources employing convex programming techniques [14]. Through the convex aproach it is relatively easy to introduce a constraint to the side-lobe-level of the radiated pattern or a limit to the minimum directivity to achieve [15].

Once the calculation is finished, we can "deflate" the inflated sources to find for each one of the sets the position

This paper has been supported in part by the MIUR program "Dipartimenti di Eccellenza 2018-2022"

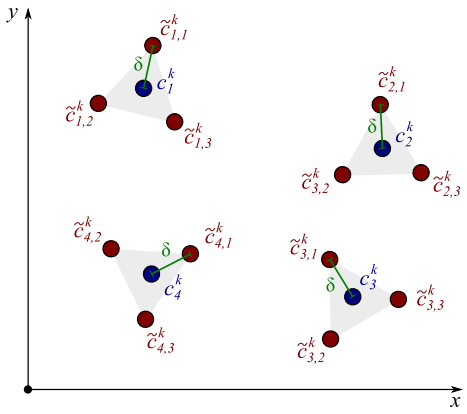

Fig. 1. Example scheme of the sources of excitation $\mathbf{c}^k$ (dark blue), and their "inflated" sources $\tilde{\mathbf{c}}^k$ (dark red) in a simple case of $N = 4$ and $P = 3$.

and excitation of a new source, of coordinates $(x_n^{k+1}; y_n^{k+1})$ and excitation c_n^{k+1}, by means of the following formulas:

$$c_n^{k+1} = \sum_{p=1}^{P} \tilde{c}_{n,p}^k \tag{3}$$

$$x_n^{k+1} = \sum_{p=1}^{P} \tilde{x}_{n,p}^k (\tilde{c}_{n,p}^k / c_n^{k+1}) \tag{4}$$

$$y_n^{k+1} = \sum_{p=1}^{P} \tilde{y}_{n,p}^k (\tilde{c}_{n,p}^k / c_n^{k+1}) \tag{5}$$

According to the specific "convex optimization" performed, the N sources will be moved, and their relative excitation will change. In I-IDEA, we exploit the equalizing property of the ℓ_2 norm, which has the advantageous feature of "pushing" the solution towards the minimum of the excitation dynamic.

Observing (3), we notice that the amplitude of the excitation of the deflated source is the sum of the excitations of the inflated set of sources. Because of this relationship we can write

$$|{c_n}^{k+1}|^2 = \left(\sum_{p=1}^{P} \tilde{c}_{n,p}^k\right)^* \left(\sum_{p=1}^{P} \tilde{c}_{n,p}^k\right) = (\tilde{\mathbf{c}}_\mathbf{n}^\mathbf{k})^\dagger \mathbf{U} (\tilde{\mathbf{c}}_\mathbf{n}^\mathbf{k}) \tag{6}$$

where, for $P = 3$, we have

$$\tilde{\mathbf{c}}_n^k = \begin{bmatrix} \tilde{c}_{n,1}^k \\ \tilde{c}_{n,2}^k \\ \tilde{c}_{n,3}^k \end{bmatrix} \quad \text{and} \quad \mathbf{U} = \begin{bmatrix} 1 & 1 & 1 \\ 1 & 1 & 1 \\ 1 & 1 & 1 \end{bmatrix} \tag{7}$$

According to this consideration, in the "convex optimization" we could then perform the minimization of the following quantity:

$$(\tilde{\mathbf{c}}^k)^\dagger \mathcal{P} \tilde{\mathbf{c}}^k \tag{8}$$

where $(\tilde{\mathbf{c}}^k)$ is a column vector collecting all the excitations of the inflated array, and $\mathcal{P}$ is a block diagonal matrix whose diagonal elements are the $\mathbf{U}$ matrices defined in (7):

$$\mathcal{P} = \begin{bmatrix} 1\,1\,1\,0\,0\,0 & & 0\,0\,0 \\ 1\,1\,1\,0\,0\,0 & \cdots & 0\,0\,0 \\ 1\,1\,1\,0\,0\,0 & & 0\,0\,0 \\ 0\,0\,0\,1\,1\,1 & & 0\,0\,0 \\ 0\,0\,0\,1\,1\,1 & \cdots & 0\,0\,0 \\ 0\,0\,0\,1\,1\,1 & & 0\,0\,0 \\ \vdots & \ddots & \vdots \\ 0\,0\,0\,0\,0\,0 & & 1\,1\,1 \\ 0\,0\,0\,0\,0\,0 & \cdots & 1\,1\,1 \\ 0\,0\,0\,0\,0\,0 & & 1\,1\,1 \end{bmatrix} \tag{9}$$

since

$$(\tilde{\mathbf{c}}^k)^\dagger \mathcal{P} \tilde{\mathbf{c}}^k = \|\mathbf{c}^{k+1}\|_2 \tag{10}$$

As it will become clear in the examples section, minimizing (8) in the convex optimization, the sources are moved at each step in order to progressively reduce the excitation dynamic. To quantify this reduction, we can introduce the excitation spread, defined as the standard deviation of $\mathbf{c}^{k+1}$ normalized to its mean and calculated as:

$$\sigma(\mathbf{c}) = N_k \sqrt{\frac{\sum_{n=1}^{N_k} (c_n - 1/N_k)^2}{N_k - 1}} \tag{11}$$

We will say that the algorithm has reached an isophoric solution when

$$\sigma(\mathbf{c}^{k+1}) \leq \sigma_T \tag{12}$$

with σ_T a threshold that has to be chosen according to the synthesis specification (we usually consider $\sigma_T = 10^{-3}$).

III. Solution Refinement

The solution refinement will be performed when an equal amplitude excitation has already been found, with the specific aim to improve the scanning performance of the antenna arrays.

This effect is obtained minimizing the power radiated in directions different from the desired one. In particular, it is essential to properly limit the radiated power resulting from different configurations of side-lobes that could be radiated by the array when the beam is scanned. Failing in this task could lead to an intense loss in directivity in non-broadside directions [15].

We can introduce the quantity $\mathcal{T}_{SLL}$, the square of the ℓ_2 norm of the array factor in the SLL region, also including part of the "invisible range" of the radiation pattern, defined as:

$$\mathcal{T}_{SLL} = \iint_{w_1 \leq \sqrt{u^2+v^2} \leq 1+w_s} |AF(u,v)|^2 \partial u \partial v \tag{13}$$

where w_1 is the pencil beam footprint and $w_s = \sin\theta_s$ with θ_s the maximum scanning angle relative to the broadside direction.

Because of the linearity of the radiation operator with respect to the inflated excitation vector $\tilde{\mathbf{c}}$, we can find a semidefinite-positive matrix $\widehat{\mathbf{\Sigma}}$ so that

$$\mathcal{T}_{SLL} = (\tilde{\mathbf{c}}^k)^\dagger \widehat{\mathbf{\Sigma}} \tilde{\mathbf{c}} \tag{14}$$

It is then straightforward to add in the convex optimization a further constraint on the quantity $\mathcal{T}_{SLL}$ in (14) to limit the

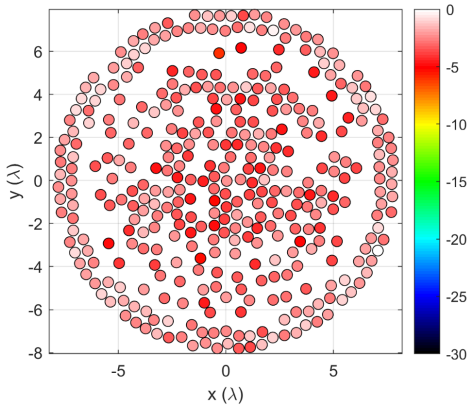

Fig. 2. The 370 elements sparse layout in [15]. The color of the circles is related to the relative amplitude of the excitations. Circles of $\lambda/2$ diameters are used in the plot to verify the non-overlapping of the sources graphically.

field radiated in the unwanted directions of all the possible steered beams:

$$(\tilde{\mathbf{c}}^k)^\dagger \widehat{\mathbf{\Sigma}} \tilde{\mathbf{c}}^k \leq \widehat{T}_k \tag{15}$$

The key point of the solution refinement is to gradually reduce the threshold $\widehat{T}_k$ according to the rule

$$\widehat{T}_k = \widehat{T}_{k-1}/(1+\alpha) \tag{16}$$

with α a small positive constant ($\alpha << 1$), in order to force the norm of the Array Factor in the SLL region to be a little smaller, thus improving the directivity of the scanned beam.

The introduction in the convex optimization of a more stringent constraint (15) will result in the excitation spreading rising, but I-IDEA will move the sources to reduce the excitation spread again.

When the excitation spread will be again lower that the chosen threshold σ_T, the quantity $\widehat{T}_k$ will be lowered again according to (16).

The rationale of this procedure is gradually achieving the minimum of (14), maintaining the isophoric property of the found solution.

IV. Synthesis Example

We will now analyze an example to understand how to implement and effectively use the approach presented in the previous sections; to this aim, we will focus only on optimizing an already synthesized array. In particular, we will optimize the excitation dynamic a $N = 370$ isotropic elements array analyzed in [15], able to radiate a broadside pattern with directivity of 29dB and with a SLL lower than -20dB for $0.067 \leq \sqrt{u^2+v^2} \leq 1.77$, so that its pattern can be scanned up to an angle of $50°$(deg) with respect to the broadside radiation for any angle ϕ without the increase of the SLL in the visible range. It is worth underlining that the excitations of the radiating elements of the array mentioned above are not uniform, and their dynamic is about 6.7dB: we want to achieve an equal amplitude solution, maintaining good scanning performances.

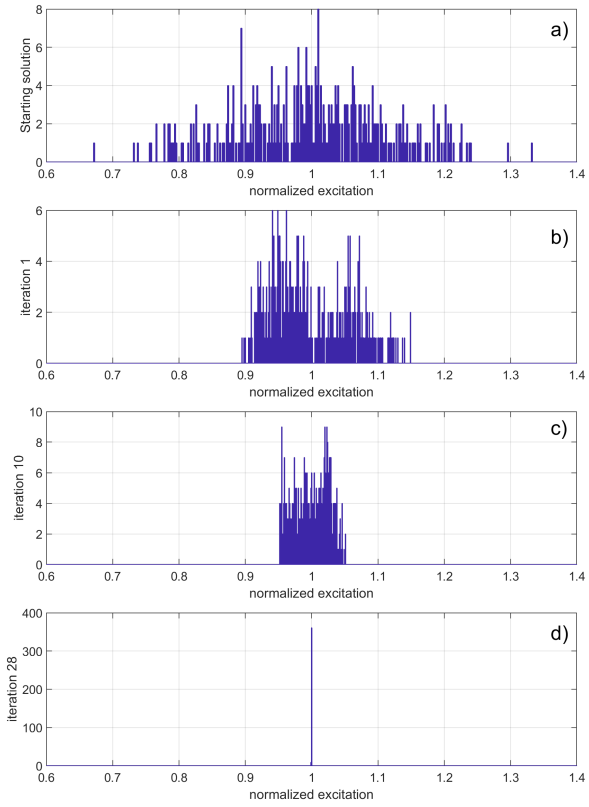

Fig. 3. Histogram of the excitation amplitude for some relevant iterations. The width of the bins for the histogram is 0.01.

Isophoric-IDEA is very effective in reducing the excitation dynamic of the source: in Fig.3 we can see the evolution of the distribution of the amplitude of the excitations $\mathbf{c}^k$ for the starting array [15] and for some relevant iterations $k = [1, 10, 28]$. In particular, the first phase of I-IDEA ends at the iteration $k = 28$, since this is the first iteration for which (12) is verified, and we can see that the histogram is collapsed in a single bin.

To better quantify the algorithm's behavior, in Fig. 4, we plot some relevant parameters as a function of the iterations. In particular the we can see that the excitation spread and the excitation dynamic Λ (the ratio of the maximum and minimum excitation amplitudes) monotonically reduces up to iteration $k = 28$, when $\sigma(\tilde{\mathbf{c}}) = 2.7 \times 10^{-4}$ and $\Lambda = 0.009$dB. Less than one hour of calculation time on a PC with an Intel i7-8700k processor and 32GB RAM was required to achieve this solution using Matlab, and CVX [16].

From Fig.4 we can also see the behavior of $\mathcal{T}_{SLL}$, the quadratic functional introduced in (14), and we can see that this quantity slightly increases during the iterations: if we calculate the directivity of the most scanned pattern for the layout at $k = 28$, we will get a slightly lower value with respect to the starting layout (25.9dB instead of 26.0dB of [15]).

From Fig.4 we can also see the parameters of the synthesis for iterations $k > 28$, when the refinement phase of I-IDEA

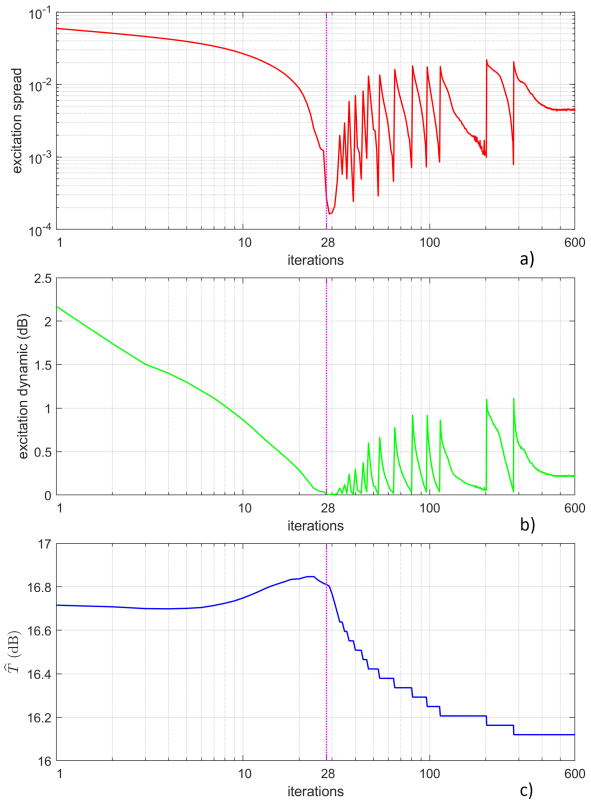

Fig. 4. Variation of some relevant parameters for a variable iteration. Iteration $k = 28$ is marked with a vertical magenta line to emphasize the switching of the optimization algorithm.

starts, using $\alpha = 0.01$. Apart from the first few iterations, the excitation spread and dynamic excitation start to show an oscillatory behavior: when the threshold on $\mathcal{T}_{SLL}$ is lowered according to (16), the excitation spread exceeds the threshold (12), and then it reduces again, in a process that leads to the reduction of the norm of the field out of the main beam. This oscillatory behavior ends when the threshold on $\mathcal{T}_{SLL}$ is so low that the excitation spread cannot go below σ_T. As it is clear from the plots in Fig.4, the first part of the refinement, say up to $k \approx 100$ is relatively quick, then the algorithm requires a large number of iterations to further reduce the norm of the field in unwanted directions. In this particular case, we truncated the execution at $k = 600$, after about 20h of computation, only to help the reader understand the behavior of the algorithm in its final stage. However, it is generally of little engineering interest to reach this amount of iterations. After the refinement, the directivity of the most scanned beam is about 26.1dB, slightly larger than the one of the starting array. We have obtained an array with equal excitation amplitudes that achieves an even better directivity with respect to the non-equal amplitude array.

The final layout is shown in Fig.5. It must be underlined that the minimum distance between the elements is greater than $\lambda/2$, and the average minimum distance between them is about 0.6λ. The radiated pattern for the broadside beam and one of

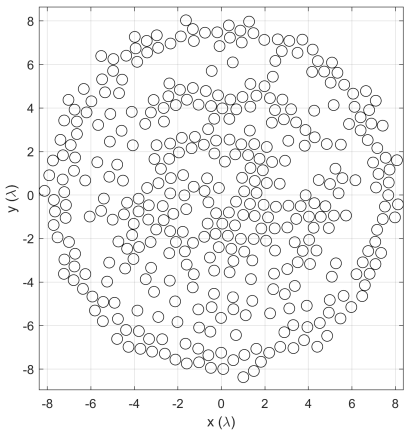

Fig. 5. Layout of the optimized array of N=370 radiating elements. Circles of $\lambda/2$ diameters are used in the plot to graphically verify the non-overlapping of the sources.

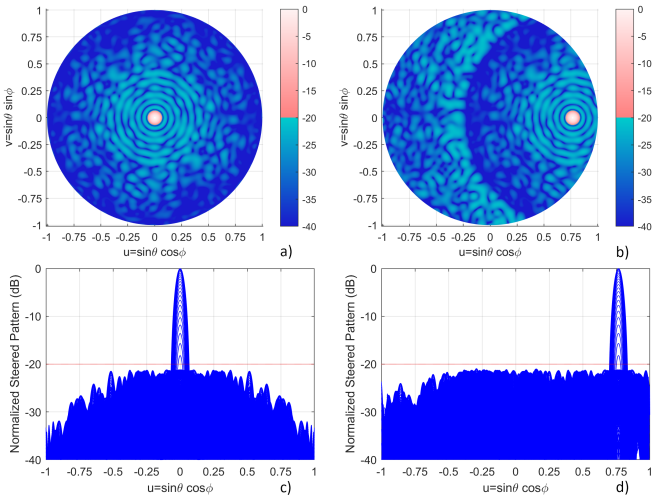

Fig. 6. Patten of the optimized array of N=370 radiating elements. On the left subplots: broadside beam; on the right subplots: one of the most scanned beams. The upper plots show the pattern employing imagemaps, the lower plots show all the cuts with constant v.

the most scanned beams is provided in Fig.6, and we can easily verify that the SLL is always lower than -21dB in the visible range for any scanned beam (a significant improvement with respect to the request of the specifications).

In Fig.7 we provide two QR codes containing in text format (not weblinks) the positions of the radiating elements of the example: in this way, any researcher could check and verify the claimed results, also using different approaches, not considered in this paper. Other data, together with some animations, are also provided on IEEE DataPort (https://dx.doi.org/10.21227/n6fx-js51). More examples will be provided during the presentation of the paper.

V. Conclusions

An effective strategy for the synthesis of isophoric sparse arrays has been presented.

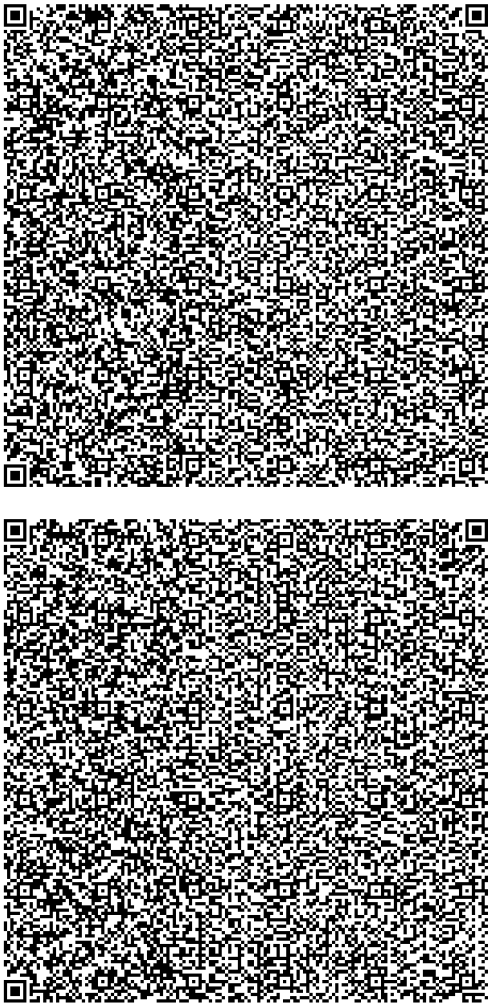

Fig. 7. QR codes containing the positions of the feeds for the optimized array of N=370 radiating elements.

Differently by concurrent approaches, in the presented method, we start from an antenna layout with non-equal amplitude excitations, and we first find a solution that verifies the wanted specifications using equal amplitude excitations; then, the solution is refined in order to improve the scanning performance.

In future development the strategy will be improved to include the effect of mutual coupling in the synthesis; moreover, shaped beam synthesis will also be considered.

ACKNOWLEDGMENT

This paper has partly been supported by the MIUR program "Dipartimenti di Eccellenza 2018-2022".

REFERENCES

[1] L. Lu, G. Y. Li, A. L. Swindlehurst, A. Ashikhmin, and R. Zhang, "An overview of massive MIMO: Benefits and challenges," *IEEE J. Sel. Topics Signal Process.*, vol. 8, no. 5, pp. 742–758, Oct. 2014.

[2] Z. Lin, Y. Chen, X. Liu, R. Jiang, B. Shen, and G. Xin-Xin, "Optimized design for sparse arrays in 3-d imaging sonar systems based on perturbed bayesian compressive sensing," *IEEE Sensors J.*, vol. 20, no. 10, pp. 5554–5565, 2020.

[3] D. Pinchera, M. D. Migliore, and F. Schettino, "Optimizing antenna arrays for spatial multiplexing: Towards 6g systems," *IEEE Access*, vol. 9, pp. 53 276–53 291, 2021.

[4] P. Rocca, G. Oliveri, R. J. Mailloux, and A. Massa, "Unconventional phased array architectures and design methodologies—a review," *Proc. IEEE*, vol. 104, no. 3, pp. 544–560, 2016.

[5] D. Dai, M. Yao, H. Ma, W. Jin, and F. Zhang, "An asymmetric mapping method for the synthesis of sparse planar arrays," *IEEE Trans. Antennas Propag.*, vol. 17, no. 1, pp. 70–73, 2017.

[6] D. Pinchera, M. D. Migliore, F. Schettino, M. Lucido, and G. Panariello, "An effective compressed-sensing inspired deterministic algorithm for sparse array synthesis," *IEEE Trans. Antennas Propag.*, vol. 66, no. 1, pp. 149–159, 2018.

[7] A. Salas-Sanchez, J. Rodriguez-Gonzalez, and F. Ares-Pena, "Hybrid method for the synthesis of isophoric phase-shaped beams," *IEEE Trans. Antennas Propag.*, vol. 66, no. 12, pp. 7439–7442, 2018.

[8] D. Pinchera, M. D. Migliore, and G. Panariello, "Synthesis of large sparse arrays using idea (inflating-deflating exploration algorithm)," *IEEE Trans. Antennas Propag.*, vol. 66, no. 9, pp. 4658–4668, 2018.

[9] P. Gu, G. Wang, Z. Fan, and R. Chen, "An efficient approach for the synthesis of large sparse planar array," *IEEE Trans. Antennas Propag.*, vol. 67, no. 12, pp. 7320–7330, 2019.

[10] P. Rocca, N. Anselmi, A. Polo, and A. Massa, "An irregular two-sizes square tiling method for the design of isophoric phased arrays," *IEEE Trans. Antennas Propag.*, vol. 68, no. 6, pp. 4437–4449, 2020.

[11] Y. Miao, F. Liu, J. Lu, and K. Li, "Synthesis of unequally spaced arrays with uniform excitation via iterative second-order cone programming," *IEEE Trans. Antennas Propag.*, vol. 68, no. 8, pp. 6013–6021, 2020.

[12] D. G. Leeper, "Isophoric arrays-massively thinned phased arrays with well-controlled sidelobes," *IEEE Trans. Antennas Propag.*, vol. 47, no. 12, pp. 1825–1835, 1999.

[13] D. Pinchera, M. D. Migliore, and G. Panariello, "Isophoric inflating deflating exploration algorithm (i-idea) for equal-amplitude aperiodic arrays," *IEEE Transactions on Antennas and Propagation*, 2022, in press (online available).

[14] H. Lebret and S. Boyd, "Antenna array pattern synthesis via convex optimization," *IEEE transactions on signal processing*, vol. 45, no. 3, pp. 526–532, 1997.

[15] D. Pinchera, "On the trade-off between the main parameters of planar antenna arrays," *Electronics*, vol. 9, no. 5, p. 739, 2020.

[16] "Cvx: Matlab software for disciplined convex programming," accessed: 2021-11-17. [Online]. Available: http://cvxr.com/cvx/